

Natarajan Thiruvani<sup>1,2</sup>, Ramu Mathamma<sup>2</sup>, Dhanapal Prakash Babu<sup>3</sup>, Sadasivam Ponkumar<sup>4</sup>, Ramasamy Jayavel<sup>5</sup>

<sup>1</sup>Department of Physics, Government Arts College for Women, Salem, India, <sup>2</sup>Department of Physics, Sri Sarada college for women (Autonomous), Salem, India, <sup>3</sup>School of Applied Sciences, Department of Physics, REVA University, Bangalore, India, <sup>4</sup>Department of Physics, Thiruvalluvar Government Arts College, Namakkal, India, <sup>5</sup>Crystal Growth Centre, Anna University, Chennai -600 025

Scientific paper

ISSN 0351-9465, E-ISSN 2466-2585

<https://doi.org/10.62638/ZasMat1133>



Zastita Materijala 65 (2)  
279 - 284 (2024)

## A novel $\text{Sr}_{0.99}\text{Zr}(\text{PO}_4)_2:0.01\text{Eu}^{3+}$ ceramic glass viable for long term energy storage applications

### ABSTRACT

This paper reports the first-time synthesis of  $\text{Sr}_{0.99}\text{Zr}(\text{PO}_4)_2:0.01\text{Eu}^{3+}$  ceramic glass were synthesized via solution combustion using glycine as fuel (1:1 fuel-to-oxidizer ratio). X-ray diffraction confirmed the desired crystalline phase, while Scherrer analysis indicated an average particle size of approximately 60 nm. This was further supported by scanning electron microscopy, which revealed a particle size around 75 nm. Notably, the material exhibited a characteristic mesoporous structure, a signature feature of the solution combustion technique. Dielectric studies revealed a double exponential decay profile, signifying the presence of voids within the material. Importantly, the significantly smaller time constant ( $t_2$ ) compared to  $t_1$  highlights the material's suitability for long-term energy storage applications.

**Keywords:** SZO nanoceramics, solution combustion synthesis, energy storage, dielectric properties

### 1. INTRODUCTION

For decades, phosphates have captivated researchers due to their diverse applications, encompassing everything from phosphors and nuclear waste forms to thermal barrier coatings, catalysts, and solid electrolytes [1]. These materials boast remarkable characteristics, including exceptional chemical stability, low thermal conductivity, high melting points, a high thermal expansion coefficient, and the ability to readily accommodate defects [2]. Recently, zirconia-based materials have attracted significant attention for their potential as energy storage materials. This surge in interest on  $\text{Eu}^{3+}$  doped materials has spurred extensive research into their preparation and functional properties, leading to the development of diverse synthesis methods like solid-state reaction, sol-gel, combustion, stearic acid, solution combustion, and hydrothermal techniques [3].

While solid-state synthesis remains popular due to its simplicity, its limitations, such as high temperatures (often exceeding 1200°C) and lengthy reaction times (lasting several days), can lead to large agglomerates [4].

Building upon our previous success in overcoming limitations like high temperatures and long reaction times through solution combustion [5], this work delves deeper into the preparation and characterization of  $\text{Sr}_{0.99}\text{Zr}(\text{PO}_4)_2:0.01\text{Eu}^{3+}$  nanopowders. This efficient route yielded materials with a desirable mesoporous structure and enhanced chemical homogeneity, paving the way for simpler and more cost-effective synthesis compared to traditional methods. Here, we focus on comprehensively understanding these promising materials, paving the way for their potential applications in energy storage of  $\text{Sr}_{0.99}\text{Zr}(\text{PO}_4)_2:0.01\text{Eu}^{3+}$ .

Driven by the pressing need for efficient, durable, sustainable, and affordable energy storage solutions [7], researchers are exploring novel materials with exceptional properties. Supercapacitors, bridging the gap between capacitors and batteries, offer promising possibilities for applications requiring rapid energy cycling due to their fast charging/discharging capabilities [8]. This has sparked significant interest

\*Corresponding author: Natarajan Thiruvani

E-mail: [thiruvaninatarajan23@gmail.com](mailto:thiruvaninatarajan23@gmail.com)

Paper received: 15. 12. 2023.

Paper accepted: 26.12.2023.

Paper is available on the website: [www.idk.org.rs/journal](http://www.idk.org.rs/journal)

in materials with supercapacitive potential. Preliminary studies suggest that  $\text{SrZr}(\text{PO}_4)_2$  exhibits promising supercapacitive properties and corrosion protection coatings [9], making it a prime candidate for further exploration and optimization.

Its unique combination of desirable properties, including high stability, low thermal expansion, and superionic conductivity [10, 11], makes it an attractive candidate for various technological advancements. Continued research and development are crucial to unlock the full potential of  $\text{SrZr}(\text{PO}_4)_2$  and contribute to the advancement of diverse industries [12].

Orthophosphates have emerged as prominent host materials for dielectric applications due to their exceptional properties, including a large band gap, moderate phonon energy and high chemical stability [13].  $\text{Sr}_{0.99}\text{Zr}(\text{PO}_4)_2:0.01\text{Eu}^{3+}$  ceramic material was specifically chosen for this study due to its advantageous characteristics:

- Ionic conductivity: Facilitates efficient charge transport.
- Anisotropy: Enables tailoring material properties for specific applications.
- Lower thermal expansion: Enhances material stability [13].
- Larger ionic radii: Allows effective incorporation of rare-earth ions without altering the crystal structure [14].
- Presence of zirconium and phosphate: Provides a well-defined crystal field for structural applications.

Despite the promising potential of  $\text{SrZr}(\text{PO}_4)_2$ , limited research has been conducted on its dielectric properties, particularly regarding  $\text{Eu}^{3+}$  doping. This work aims to address this gap by exploring dielectric properties of this material. To

the best of our knowledge, no reports are available on these specific aspects of  $\text{Sr}_{0.99}\text{Zr}(\text{PO}_4)_2:0.01\text{Eu}^{3+}$ .

**Significance of the Study:** This study ventures into the uncharted territory of  $\text{Sr}_{0.99}\text{Zr}(\text{PO}_4)_2:0.01\text{Eu}^{3+}$ 's dielectric properties, shedding light on its potential for innovative technological advancements. Unveiling its dielectric behavior offers valuable insights into the material's suitability for specific applications.

## 2. PREPARATION:

$\text{Sr}_{0.99}\text{Zr}(\text{PO}_4)_2:0.01\text{Eu}^{3+}$  was prepared by solution combustion method with F/O ratio maintained at unity. Stoichiometric amounts of  $\text{ZrO}(\text{NO}_3)_2$ ,  $\text{NH}_6(\text{PO}_4)_2$ ,  $\text{Eu}(\text{NO}_3)_3$ ,  $\text{Sr}(\text{NO}_3)_2$ , and Glycine were dissolved in 50 ml of double distilled water to obtain a homogenous solution. The precursor solution was then transferred to a crystalline dish and placed in a preheated muffle furnace at  $500^\circ\text{C}$ . Upon completion of the reaction, the sample was removed from the furnace and allowed to cool to room temperature. Finally, the powder was calcined at  $800^\circ\text{C}$  for 6 hours.

## 3. RESULT AND DISCUSSION

### 3.1. XRD analysis

To ascertain the crystallinity, phase purity, and structural information of  $\text{Sr}_{0.99}\text{Zr}(\text{PO}_4)_2:0.01\text{Eu}^{3+}$ , powder X-ray diffraction (XRD) measurements were conducted, Fig. 1. The observed diffraction patterns aligned well with ICSD file number 150336 [14]. The crystalline sizes of the prepared samples were calculated using the Scherer method and were about 60nm.

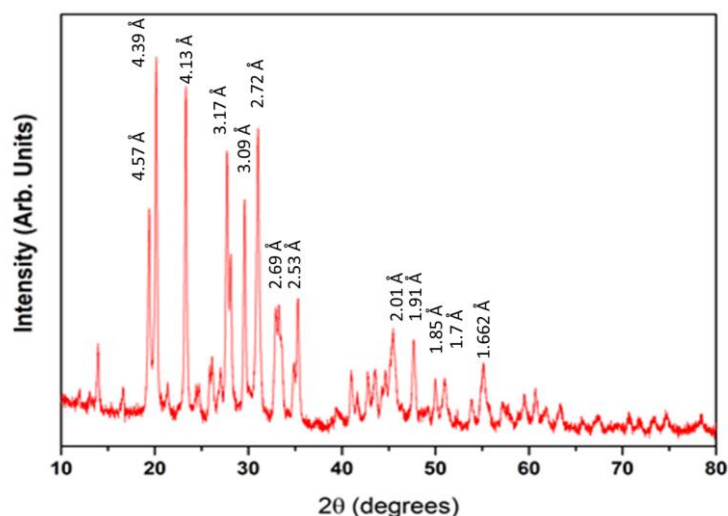


Figure 1. PXR D spectrum of  $\text{Sr}_{0.99}\text{Zr}(\text{PO}_4)_2:0.01\text{Eu}$

Slika 1. PXR D spektar  $\text{Sr}_{0.99}\text{Zr}(\text{PO}_4)_2:0.01\text{Eu}$

The Scherer equation is given by:

$$D = k\lambda/\beta\cos\theta \quad (1)$$

where  $\lambda$  is the wavelength of X-rays (1.5406 Å),  $\beta$  is the full width half maxima of diffraction peaks,  $k$  is the Scherer's constant (0.9), and  $\theta$  is the Bragg's angle.

### 3.3. SEM

Figure 2 presents SEM images of the sample, highlighting microstructure of the sample. This

reveal mesoporous nature of the sample with particle distribution in nano meter range. These observations can be attributed to the evolution of a substantial amount of gases during the combustion process, leading to the formation of voids and pores. The measured particle size in the SEM micrographs, around 75 nm, coincides with the results obtained from PXRD studies, suggesting consistency between the two characterization techniques.

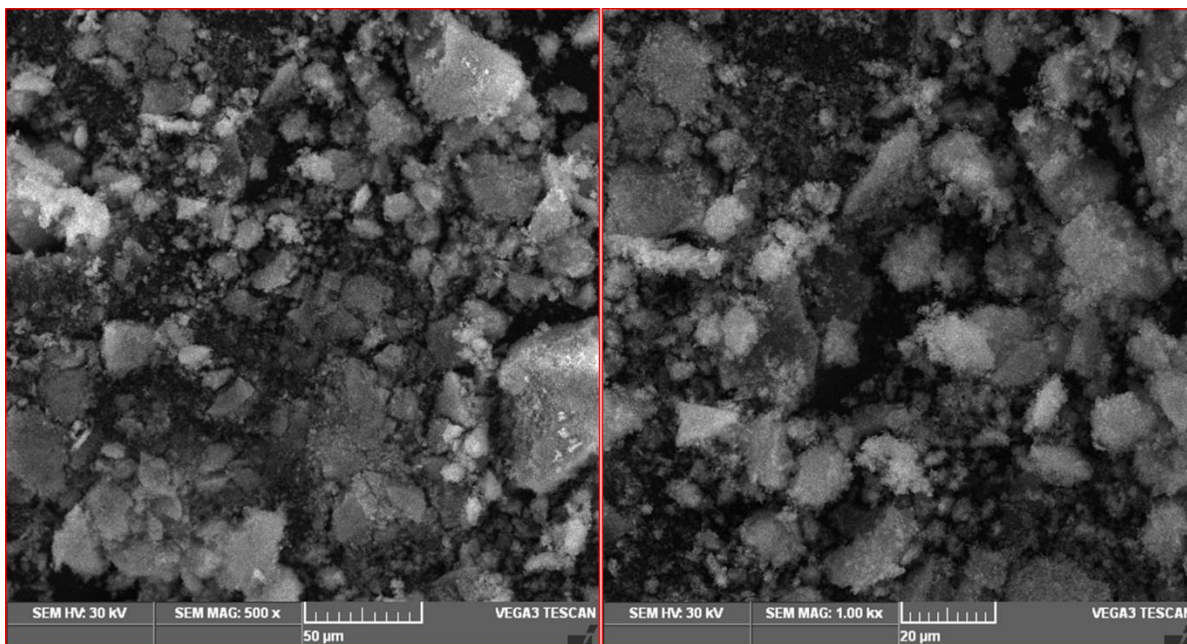


Figure 2. SEM micrograph of  $\text{Sr}_{0.99}\text{Zr}(\text{PO}_4)_2:0.01\text{Eu}$  at 50 and 20  $\mu\text{m}$  magnification

Slika 2. SEM mikrofografija  $\text{Sr}_{0.99}\text{Zr}(\text{PO}_4)_2:0.01\text{Eu}$  pri uvećanju od 50 i 20  $\mu\text{m}$

### 3.4. Dielectric studies

Understanding the interplay between electric fields and materials forms the cornerstone of designing and developing materials for various applications. This interaction, governed by several key parameters, manifests in the form of dielectric properties [15].

Two crucial concepts in dielectric studies are relaxation time and correlation function. Relaxation time dictates how quickly a material responds to an applied electric field, representing the average time it takes for its internal dipoles to align with the field. A single relaxation time translates to an exponential decay of the material's polarization, while a distribution of relaxation times results in a more complex decay profile [16]. Analyzing the relaxation time sheds light on the dynamics of the dipoles and their response to external stimuli.

The correlation function, denoted by  $C(\tau)$ , mathematically quantifies the relationship between

a material's dielectric response at different times. Essentially, it measures how well the polarization at a specific moment relates to the polarization at a later one [17]. This function is calculated using dielectric relaxation data, typically involving measurements of the material's dielectric constant at various frequencies. By analyzing the frequency dependence of this constant, researchers can extract the relaxation time and subsequently calculate the correlation function, as per the provided formula [18].

$$C(\tau) = \lim_{T \rightarrow \infty} \frac{1}{T} \int_0^T \varepsilon(t) \varepsilon(t + \tau) dt \quad (6)$$

where:  $\varepsilon(t)$  is the dielectric constant of the material at time  $t$ ,  $\tau$  is the time lag between the two measurements of  $\varepsilon(t)$ ,  $T$  is the total time of the measurement

The relaxation time ( $\tau$ ) characterizes the time taken for the dielectric permittivity to decay to half its initial value following an electric field

perturbation [19]. Its relationship to the correlation function, C(τ), is described by:

$$C(\tau) = \frac{1}{2} \exp\left(-\frac{\tau}{\tau_R}\right) \tag{7}$$

The decay curves were fit using the double exponential equation:

$$y = A_1 \exp\left(\frac{-x}{t_1}\right) + A_2 \exp\left(\frac{-x}{t_2}\right) + y_0 \tag{8}$$

Table 1 showcases our calculated data, while Figure 3 visually dissects the dielectric decay behavior of Sr<sub>0.99</sub>Zr(PO<sub>4</sub>)<sub>2</sub>:0.01Eu<sup>3+</sup>. Here, the blue squares (■) represent the experimental data, the

red line depicts the fitted curve, and the individual decay components are shown for analysis. In this figure, "y<sub>0</sub>" signifies the initial offset level, A<sub>1</sub> and A<sub>2</sub> represent the initial amplitudes of the two exponential decay components, τ<sub>1</sub> and τ<sub>2</sub> are the time constants reflecting the decay time for each component, and k<sub>1</sub> and k<sub>2</sub> are the respective rate constants.

τ<sub>1</sub> and τ<sub>2</sub> are the time constants or decay time represented as follows:

$$\tau_1 = \frac{1}{k_1} \text{ And } \tau_2 = \frac{1}{k_2} \tag{9}$$

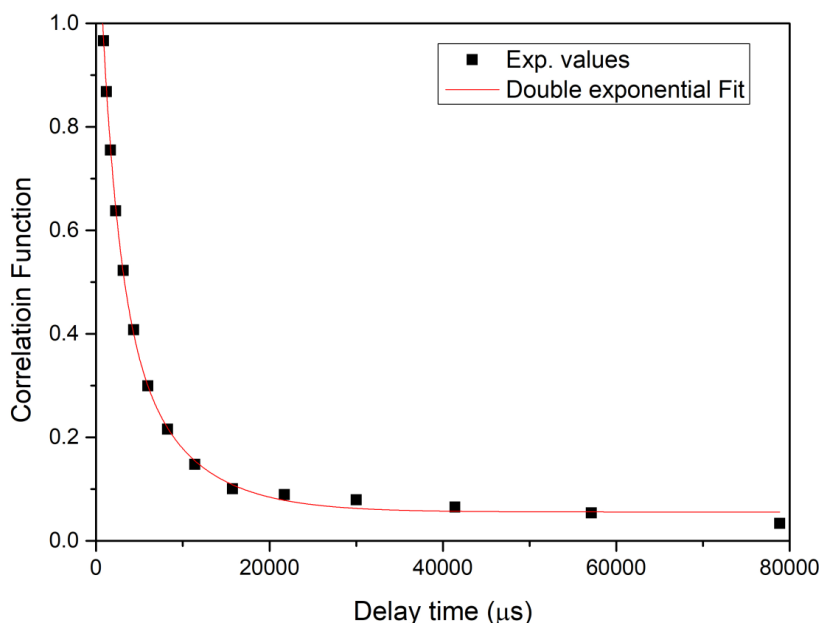


Figure3. Di-electric decay curves of Sr<sub>0.99</sub>Zr(PO<sub>4</sub>)<sub>2</sub>:0.01Eu

Slika 3. Krive dielektričnog raspada Sr<sub>0.99</sub>Zr(PO<sub>4</sub>)<sub>2</sub>:0,01Eu

Table 1. Calculated decay parameters for Sr<sub>0.99</sub>Eu<sub>0.01</sub>Zr(PO<sub>4</sub>)<sub>2</sub> by double exponential fit

Tabela 1. Izračunati parametri raspada za Sr<sub>0.99</sub>Eu<sub>0.01</sub>Zr(PO<sub>4</sub>)<sub>2</sub> dvostrukim eksponencijalnim uklapanjem

Parameter	Value
y <sub>0</sub>	0.06
A <sub>1</sub>	0.48
τ <sub>1</sub> (μs)	7078
A <sub>2</sub>	0.751
τ <sub>2</sub> (μs)	1953
k <sub>1</sub>	1.41E-04
k <sub>2</sub>	5.12E-04
τ <sub>1</sub>	4906
τ <sub>2</sub>	1354

The speed of the two exponential decay components depends on their respective time

constants. Simply put, the larger the time constant, the slower the decay. Each component's decay time is the time it takes for its signal to drop to a tiny fraction (about 0.693) of its initial strength [20].

This double-decay behavior, a hallmark of bi-exponential decay, indicates the material stores energy at two different rates. This can be attributed to the presence of two distinct mechanisms for storing charge within the material [21].

- Fast decay (t<sub>2</sub>): This rapid decline reflects the release of energy stored in the material's pores, as seen in the SEM images.
- Slow decay (t<sub>1</sub>): This slower decline corresponds to the release of energy stored deeper within the material, in its bulk.

Importantly, the much smaller value of t<sub>2</sub> compared to t<sub>1</sub> in our studies suggests this material is promising for long-term energy storage applications [22].

#### 4. CONCLUSION

For the first time, we report the synthesis of Sr<sub>0.99</sub>Zr(PO<sub>4</sub>)<sub>2</sub>:0.01Eu<sup>3+</sup> using a simple solution combustion method. XRD analysis confirms the triclinic phase of the synthesized materials, with particle sizes about 60 nm. SEM micrographs show mesoporous particle formation with lot of voids and agglomeration. Di-electric studies reveal double exponential nature of decay, confirming the presence of voids in the system. In the present studies  $t_2$  is much smaller than  $t_1$ , implying suitability of the material for long-term energy storage applications.

#### Author Contribution

All authors contributed to the study conception and design. Material preparation, data collection and analysis were performed by N. Thiruvani, R. Mathammal, S. Ponkumar, D. PrakashBabu. R. Jayavel

#### Declaration of competing interest

The authors declare that they have no known competing financial interest of personal relationships that could have appeared to influence the work reported in this paper.

#### Data Availability statement

The data that support the findings of this study are available from the corresponding author, upon reasonable request.

#### Declaration of generative AI and AI-assisted technologies in the writing process

During the preparation of this work the author(s) used Bard.ai in order to remove typo errors. After using this tool/service, the author(s) reviewed and edited the content as needed and take(s) full responsibility for the content of the publication.

#### 5. REFERENCE

- [1] K. Munirathnam, G. R. Dillip, B. D. P. Raju, S. W. Joo, S. J. Dhoble, B. M. Nagabhushana, R. Hari Krishna, K. P. Ramesh, S. Varadharaj Perumal, D. Prakashbabu (2015) Synthesis, photoluminescence and Judd–Ofelt parameters of LiNa<sub>3</sub>P<sub>2</sub>O<sub>7</sub>: Eu<sup>3+</sup> orthorhombic microstructures. *Applied Physics A*, 120, 1615–1623. <https://doi.org/10.1007/s00339-015-9371-1>
- [2] J. Fojt, L. Joska, L. Cvrček, V. Březina (2013) ZrO coatings for bioapplication. *KOM–Corrosion and Material Protection Journal*, 57(4), 93–98. <https://doi.org/10.2478/kom-2013-001>
- [3] B. Glorieux, V. Jubera, A. I. Orlova, A. E. Kanunov, A. Garcia, C. Pallier, T. A. Oleneva (2013) Phosphors based on NaZr<sub>2</sub>(PO<sub>4</sub>)<sub>3</sub>-type calcium and strontium phosphates activated with Eu<sup>2+</sup> and Sm<sup>3+</sup>. *Inorganic Materials*, 49, 82–88. <https://doi.org/10.1134/S0020168513010032>
- [4] M. Muralimanokar, V. R. Vaira, R. Padmanaban, P. G. Suganya (2020) Characterization of AZ31-NbC surface composite fabricated by friction stir processing. *KOM–Corrosion and Material Protection Journal*, 64(1), 29–37. <https://doi.org/10.2478/kom-2020-0005>
- [5] Y. H. Mohan Prakash, D. Prakash Babu, M. Madesh Kumar, S. Ponkumar, K. M. Rahulan (2021) Orange photoluminescence emission of samarium ion doped in calcium zirconium orthophosphate. *Spectroscopy Letters*, 54(4), 292–298. <https://doi.org/10.1080/00387010.2021.1930923>
- [6] D. Prakashbabu, R. H. Krishna, B. M. Nagabhushana, H. Nagabhushana, C. Shivakumara, R. P. S. Chakradar, H. B. Ramalingam, S. C. Sharma, R. Chandramohan (2014) Low temperature synthesis of pure cubic ZrO<sub>2</sub> nanopowder: Structural and luminescence studies. *Spectrochimica Acta Part A: Molecular and Biomolecular Spectroscopy*, 122, 216–222. <https://doi.org/10.1016/j.saa.2013.11.043>
- [7] F. Tudorache, K. Popa, L. Mitoseriu, N. Lupu, D. Bregiroux, G. Wallez (2011) Dielectric investigation of MIIMIV(PO<sub>4</sub>)<sub>2</sub> double orthophosphates (MI= Ca, Sr, Ba, Pb; MIV= Ti, Zr, Hf, Ge, Sn). *Journal of Alloys and Compounds*, 509(37), 9127–9132. <https://doi.org/10.1016/j.jallcom.2011.06.072>
- [8] D. Prakash Babu, S. Ponkumar (2023) Uv Irradiation Induced Capacitance Enhancement in Pani/SrZr(Po4)2 Composite. Available at SSRN: <https://ssrn.com/abstract=4575454> or <http://dx.doi.org/10.2139/ssrn.4575454>
- [9] K. Fukuda, T. Iwata, A. Moriyama, S. Hashimoto (2006) Crystal structures and phase transitions of SrZr(PO<sub>4</sub>)<sub>2</sub>–BaZr(PO<sub>4</sub>)<sub>2</sub> solid solutions. *Journal of Solid State Chemistry*, 179(12), 3870–3876. <https://doi.org/10.1016/j.jssc.2006.08.024>
- [10] Y. H. Mohan Prakash, D. Prakash Babu, M. Madesh Kumar, S. Ponkumar, K. M. Rahulan (2021) Orange photoluminescence emission of samarium ion doped in calcium zirconium orthophosphate. *Spectroscopy Letters*, 54(4), 292–298. <https://doi.org/10.1080/00387010.2021.1930923>
- [11] V. D. Sharma, P. Khajuria, S. Kumar, R. Prakash, R. J. Choudhary (2023) A novel yellow whitish Dy<sup>3+</sup> activated NaZr<sub>2</sub>(PO<sub>4</sub>)<sub>3</sub> phosphor: Structural, spectral and optical investigations. *Optik*, 291, 171354. <https://doi.org/10.1016/j.ijleo.2023.171354>
- [12] Y. Liu, M. S. Molokeev, Q. Liu, Z. Xia (2018) Crystal structures, phase transitions and thermal expansion properties of NaZr<sub>2</sub>(PO<sub>4</sub>)<sub>3</sub>–SrZr<sub>4</sub>(PO<sub>4</sub>)<sub>6</sub> solid solutions. *Inorganic Chemistry Frontiers*, 5(3), 619–625. <https://doi.org/10.1039/C7QI00782E>
- [13] D. Kajánek, B. Hadzima, F. Pastorek, M. N. Jacková (2018) Evolution of the dicalcium phosphate-dihydrate (DCPD) coating created by large amplitude sinusoidal voltammetry (LASV) on corrosion resistance of the ZW3 magnesium alloy in chloride containing environment. *KOM–Corrosion and Material Protection Journal*, 62(1), 14–18. <https://doi.org/10.2478/kom-2018-0003>
- [14] K. Fukuda, A. Moriyama, S. Hashimoto (2004) Crystal structure and phase transitions of strontium zirconium diorthophosphate, SrZr(PO<sub>4</sub>)<sub>2</sub>. *Journal of Solid State Chemistry*, 177(10), 3514–3521. <https://doi.org/10.1016/j.jssc.2004.06.002>

- [15] J.M.Arroyo, M.G.S. Rao, M.S. de U.Ventura, M.-L.T.B.Daunis, O.Rodríguez, J.W.P.Hsu, R.R.Bon (2023) All solution-processed hafnium rich hybrid dielectrics for hysteresis free metal-oxide thin-film transistors. *Journal of Materials Chemistry C*, 11(5), 1824–1841. <https://doi.org/10.1039/D2TC03761K>
- [16] W. Zhou, G. Cao, M. Yuan, S. Zhong, Y. Wang, X. Liu, D. Cao et al. (2023) Core–shell engineering of conductive fillers toward enhanced dielectric properties: a universal polarization mechanism in polymer conductor composites. *Advanced Materials*, 35(2), 2207829. <https://doi.org/10.1002/adma.202207829>
- [17] S. Sahoo, M. Bhuyan, D. Sahoo (2023) Tuning of dielectric and magnetic performance of graphene oxide via defect regulation by metal oxide nanoparticle for high temperature device. *Journal of Alloys and Compounds*, 935, 168097. <https://doi.org/10.1016/j.jallcom.2022.168097>
- [18] L.M.Al-Harbi, Q.A.Alsulami, M.O.Farea, A.Rajeh (2023) Tuning optical, dielectric, and electrical properties of Polyethylene oxide/Carboxymethyl cellulose doped with mixed metal oxide nanoparticles for flexible electronic devices. *Journal of Molecular Structure*, 1272, 134244. <https://doi.org/10.1016/j.molstruc.2022.134244>
- [19] S.J.Rzoska, A.Drozd-Rzoska, W.Bulejak, J.Los, S.Starzonek, M.Szafran, F.Gao (2023) A Critical Insight into Pretransitional Behavior and Dielectric Tunability of Relaxor Ceramics. *arXiv preprint arXiv:2310.13326*. <https://doi.org/10.3390/ma16247634>
- [20] O.I.Sallam, M.M.Atta, E.O.Taha, A.M. Elbasiony, A.M.A.Henaish, R.M.Ahmed (2023) Synthesis and modification of photoluminescence and dielectric properties of novel fluorophosphate glass by incorporating different transition metal oxides for optoelectronic applications. *Optical Materials*, 136, 113413. <https://doi.org/10.1016/j.optmat.2022.113413>
- [21] K.G.Mondal, B.S.Kar, S.Rakshit, S. Saha, P.C.Jana, M.N.Goswami (2023) Optical, structural and dielectric properties of solvothermally grown molybdenum sulfide nanosheets. *Journal of Alloys and Compounds*, 969, 172356. <https://doi.org/10.1016/j.jallcom.2023.172356>
- [22] W. Xu, Y. Li, Q. Cui, H. Zhang, C. Xia, H. Guo, G. Zhou (2023) All-optical generation, detection, and manipulation of picosecond acoustic pulses in 2D semiconductor/dielectric heterostructures. *Photonics Research*, 11(12), 2000–2010. <https://doi.org/10.1364/PRJ.491805>

## IZVOD

### NOVO $\text{Sr}_{0.99}\text{Zr}(\text{PO}_4)_2:0.01\text{Eu}^{3+}$ KERAMIČKO STAKLO ODRŽIVO ZA DUGOROČNE APLIKACIJE ZA SKLADIŠTENJE ENERGIJE

*U ovom radu je prikazana prva sinteza  $\text{Sr}_{0.99}\text{Zr}(\text{PO}_4)_2:0.01\text{Eu}^{3+}$  keramičkog stakla sintetizovana sagorevanjem rastvora korišćenjem glicina kao goriva (odnos goriva i oksidatora 1:1). Difrakcija rendgenskih zraka je potvrdila željenu kristalnu fazu, dok je Šererova analiza pokazala prosečnu veličinu čestica od približno 60 nm. Ovo je dodatno podržano skenirajućim elektronskim mikroskopom, koji je otkrio veličinu čestica oko 75 nm. Primetno je da je materijal pokazao karakterističnu mezoporoznu strukturu, prepoznatljivu karakteristiku tehnike sagorevanja rastvora. Dielektrične studije su otkrile dvostruki eksponencijalni profil raspadanja, što označava prisustvo praznina unutar materijala. Važno je da značajno manja vremenska konstanta ( $t_2$ ) u poređenju sa  $t_1$  naglašava pogodnost materijala za dugoročne aplikacije za skladištenje energije.*

**Ključne reči:** SZO nanokeramika, sinteza sagorevanja rastvora, skladište energije, dielektrična svojstva.

*Naučni rad*

*Rad primljen: 15.12.2023.*

*Rad prihvaćen: 26.12.2023.*

*Rad je dostupan na sajtu: [www.idk.org.rs/casopis](http://www.idk.org.rs/casopis)*